Journal of Materials Chemistry C

ROYAL SOCIETY OF CHEMISTRY

PAPER

View Article Online
View Journal

Cite this: DOI: 10.1039/d6tc00432f

Disorder stabilisation of high pressure $Mn_{2-x}Co_xScSbO_6$ double perovskites with complex magnetic properties

K. Ji,*[ab] F. Denis Romero,[a] C. Ritter,[c] J. Paul Attfield [b] and Y. Shimakawa [a]

Received 9th February 2026,
Accepted 31st March 2026

DOI: 10.1039/d6tc00432f

rsc.li/materials-c

High-pressure synthesis provides a powerful route to stabilise metastable oxides with unconventional structural and magnetic properties. Here we show that $Mn_{2-x}Co_xScSbO_6$ (x = 0.5, 1 and 1.5) solid solutions synthesised at 6 GPa pressure form double perovskites (space group $P2_1/n$) whereas the previously-reported x = 0 and 2 end members adopt the corundum-derived Ni_3TeO_6 structure-type ($R3$) at comparable pressure. This behaviour is consistent with disorder (configurational entropy) assisted stabilisation of the $A_2BB'O_6$ double perovskite phase under the reported high-pressure synthesis conditions, and neutron diffraction reveals substantial cation disorder with approximate distribution $(Mn_{2-x}Sc_{0.5}Co_{x-0.5})(Sc_{0.5}Co_{0.5})SbO_6$ for $0.5 < x < 1.5$. The long range antiferromagnetic order previously reported for x = 0 at T_N = 22 K is increasingly suppressed by Co-doping. The x = 0.5 sample also orders antiferromagnetically (T_N = 18 K) with ordered moments rotated and reduced in magnitude relative to x = 0, but x = 1 and 1.5 exhibit probable spin-freezing transitions (at T_g = 15 and 8 K respectively) without observed long-range magnetic order. This study demonstrates that interesting new magnetic materials may be accessed through a combination of high pressure synthesis and disorder-stabilisation of mixed-cation phases.

Introduction

Complex transition metal oxides have long attracted attention for emergent phenomena arising from the strong coupling between charge, spin, orbital, and lattice degrees of freedom.[1,2] Their remarkable structural adaptability enables the stabilisation of multiple competing frameworks, most notably perovskite and corundum-derived types, which can host distinct electronic and magnetic ground states.[3,4] High-pressure high-temperature (HPHT) synthesis provides an effective route to access such metastable oxides beyond ambient condition limits.[5] Recent discoveries, including high-T_C half-metallic ferrimagnetism $CaCu_3Fe_2Re_2O_{12}$ and $NaCu_3Fe_2Os_2O_{12}$,[6,7] charge-transfer-driven colossal negative thermal expansion in $LaCu_3Fe_4O_{12}$ and $BiNiO_3$,[8,9] and pressure-stabilised polar corundum phases such as in $InVO_3$ and Mn_2MnSbO_6,[10,11] exemplify the power of HPHT techniques in revealing new compounds with unconventional functionalities. Among these, double-perovskite (DPv) and polar corundum-derived Ni_3TeO_6-type (NTO) frameworks stand out as versatile hosts for transition-metal cations. The rock-salt ordered B/B′ sublattices of DPv oxides supports diverse electronic and magnetic states, from insulating antiferromagnets to ferrimagnets and half-metals;[12–16] whereas the NTO-type lattice, with a pronounced sensitivity to cation size and valence, gives rise to exotic spin configurations, multiferroicity, and field-induced magnetic transitions.[17,18] Both frameworks are highly responsive to pressure, temperature and chemical substitution, offering fertile ground to explore how structural distortions mediate electronic and magnetic reconfigurations.[19]

Mn_2ScSbO_6 (x = 0 in the $Mn_{2-x}Co_xScSbO_6$ series) shows several polymorphs with increasing pressure. At ambient pressure it crystallises in a cation disordered structure (Mg_3TeO_6-type, $R\bar{3}$) with no long-range magnetic ordering.[20] Under HPHT synthesis at 5.5 GPa, a polar NTO-type polymorph ($R3$) forms, displaying ferrimagnetic ordering below 42 K, whereas at higher pressure (12 GPa), a B-site ordered DPv phase ($P2_1/n$) is obtained, in which the larger Mn^{2+} cations occupy the 8-coordinate A-sites, while Sc^{3+} and Sb^{5+} order over the octahedral B/B′ sublattices. This DPv polymorph exhibits antiferromagnetic ordering of Mn spins below T_N = 22 K.[21] In contrast, Co_2ScSbO_6 (x = 2) adopts only the NTO-type polar structure ($R3$) at 6 and 12 GPa pressure. Interesting magnetism is observed below T_N = 60 K as the strong single-ion anisotropy of Co^{2+} gives rise to a long-period locked-in helical spin structure coexisting with a ferrimagnetic phase.[22] Thus, in Mn_2ScSbO_6, high pressure stabilises two polymorphs that host distinct magnetic ground states, whereas Co_2ScSbO_6 crystallises

[a] Institute for Chemical Research, Kyoto University, Uji, Kyoto 611-0011, Japan. E-mail: ji.kunlang.6v@kyoto-u.ac.jp
[b] Centre for Science at Extreme Conditions (CSEC) and School of Chemistry, University of Edinburgh, Edinburgh EH9 3FD, UK
[c] Institute Laue-Langevin, 38042 Grenoble, France

solely in the NTO-type phase with complex anisotropy-driven magnetism.

These contrasting structural and magnetic behaviours raise important questions about intermediate compositions. Do they preferentially stabilise one structural motif over the other, or can hidden metastable states emerge across the solid solution? And how are magnetic ground states affected once solid solutions are formed? Addressing these questions will clarify how cation substitution mediates polymorph stabilisation and governs the potential new magnetic ground states across the solid solution system. Here we report the high-pressure synthesis and characterisation of $Mn_{2-x}Co_xScSbO_6$ solid solutions, in which the DPv polymorph is unexpectedly stabilised at low pressure, enabling direct comparison of structural and magnetic evolution across the full composition range.

Experimental

Polycrystalline specimens of $Mn_{2-x}Co_xScSbO_6$ (x = 0.5, 1 and 1.5) were synthesised under HPHT conditions. Stoichiometric amounts of MnO, CoO, Sc_2O_3 and Sb_2O_5 were ground together, packed into Pt capsules and loaded into a cubic-type press. The synthesis condition was selected to be 6 GPa and 1100 °C for 30 minutes, followed by rapid cooling and decompression to ambient conditions. The precursor of x = 1 was also heated to 1100 °C at ambient pressure (AP) using a conventional solid-state synthesis.

Phase purity and crystal structures were characterised by Rietveld refinement[23] against powder X-ray diffraction (PXD) data collected on a Bruker D8 diffractometer using Cu $K_{\alpha1}$ radiation (λ = 1.5405 Å) in Bragg–Brentano geometry. The diffractograms were collected between 10° and 80° with a step size of 0.04°.

Magnetic susceptibility measurements were performed using a Quantum Design MPMS-XL SQUID magnetometer with Zero-Field-Cooled (ZFC) and Field-Cooled (FC) conditions in the temperature range 2 K $\leq T \leq$ 300 K under an applied field of 0.1 T. ZFC and FC data under applied fields of 0.01 and 1 T were also collected for x = 1. Magnetisation data as a function of the applied magnetic field were collected at 5 and 300 K.

Neutron powder diffraction (NPD) data were collected from the HPHT samples using the D20 diffractometer at the ILL facility; with the high-resolution mode (λ = 1.54 Å, take-off angle 90°) at 300 K, 80 K and 1.5 K for crystal and magnetic structural determination for all solid solutions. Additional high flux mode (λ = 2.41 Å, take-off angle 42°) data were used for x = 0.5 to help identify the magnetic peaks. Variable temperature data in 1 K steps were collected for x = 0.5 up to 80 K. The nuclear structures were refined using Rietveld analysis[23] through the FullProf package and the magnetic symmetry analysis was performed by means of the program BasIreps.[24]

Results and discussion

Room temperature PXD data show that all $Mn_{2-x}Co_xScSbO_6$ (x = 0.5, 1 and 1.5) solid solutions synthesised at 6 GPa crystallised in a double perovskite DPv structure in monoclinic $P2_1/n$ space group, confirmed by the presence of the characteristic DPv peaks highlighted in Fig. 1a. This is in sharp contrast to the end-member compositions (x = 0 and 2) which under the same synthesis conditions adopt NTO-type structures.[21,22] Ambient pressure synthesis of x = 1 was also carried out and this yielded an $R\bar{3}$ distorted-Mg_3TeO_6 type structure (Fig. S1), which is not corundum-derived but is analogous to that of the x = 0 parent synthesised at AP.[20] An attempt to prepare the x = 2 composition at ambient condition however gave a mixture of $Co_{2.33}Sb_{0.67}O_4$ and other phases.[22]

Neutron powder diffraction data were collected from the $Mn_{2-x}Co_xScSbO_6$ (x = 0.5, 1 and 1.5) samples synthesised at 6 GPa in order to determine the cation site occupancies and oxide anion positions. High resolution data collected at 300 K from x = 0.5 in Fig. 1b and x = 1 and 1.5 in Fig. S2 (SI) confirmed the main phase is DPv $P2_1/n$ structure (~80%), with small

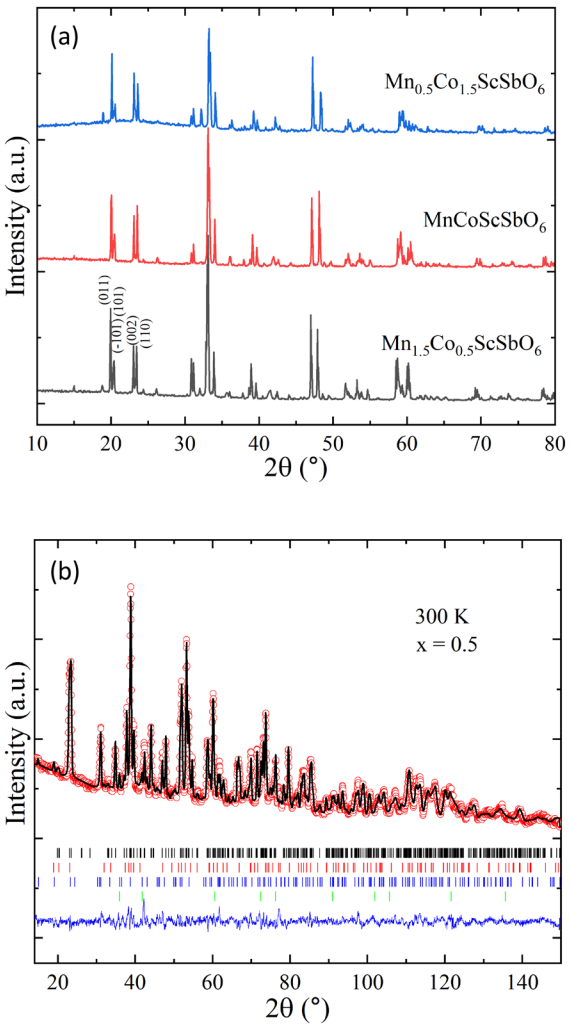

Fig. 1 (a) XRD patterns for HPHT-synthesised $Mn_{2-x}Co_xScSbO_6$ samples with nominal composition as shown. Peaks characteristic of the monoclinic $P2_1/n$ DPv structure are indexed on the lower pattern. (b) Rietveld fit to 300 K high resolution NPD data for x = 0.5. DPv-phase (80(1)%), NTO-phase (8(1)%), $Sc_{5.5}Sb_{1.5}O_{12}$ (8(1)%) and (Mn/Co)O (4(1)%) are denoted by black, red, blue and green tick marks, respectively.

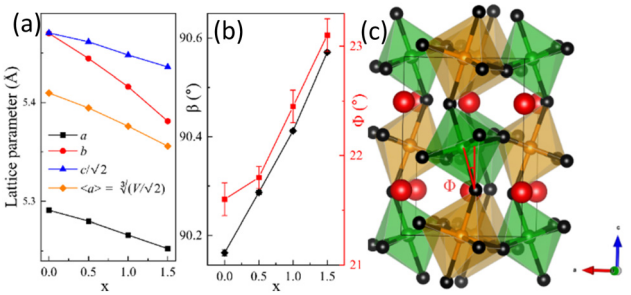

Fig. 2 (a) and (b) Lattice parameters including monoclinic angle β and octahedral tilting angle Φ changes with increasing Co-content x. Data are from 300 K NPD refinements. (c) Crystal structure of the DPv phase with Φ labelled. Red, green, orange and black spheres denote A = (Mn/Co/Sc), B = (Sc,Co), B′ = Sb and O, respectively, in the $A_2BB'O_6$ double perovskite structure.

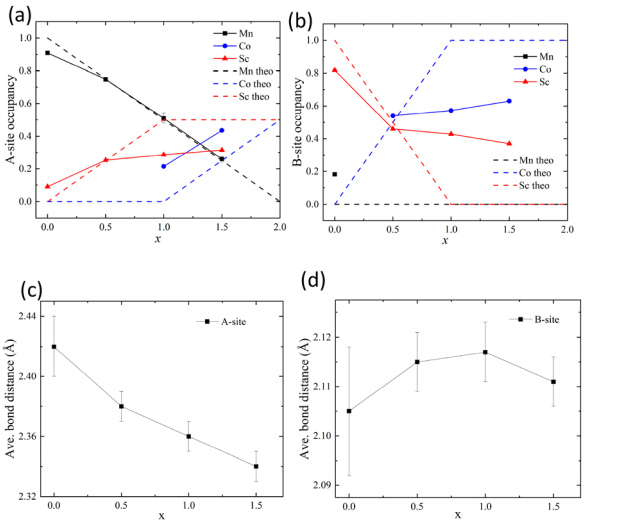

Fig. 3 Refined and theoretical (dashed lines) cation occupancy variations for (a) A-sites and (b) B-sites with x in $A_2BB'O_6$ $Mn_{2-x}Co_xScSbO_6$ double perovskite structures. Average metal to oxide bond distances are shown for (c) A-sites and (d) B-sites.

amounts of an NTO-type polymorph (~8%), $Sc_{5.5}Sb_{1.5}O_{12}$ and (Mn,Co)O as secondary phases. The refined lattice parameters in Fig. 2a decrease with increasing Co content x, consistent with substitution of larger Mn^{2+} by smaller Co^{2+}.

In the monoclinic $A_2BB'O_6$ $Mn_{2-x}Co_xScSbO_6$ DPv structures (which have $a^-a^-c^+$ octahedral tilts in Glazer notation[25]), Sc, Sb are six-fold coordinated and ordered in a rock-salt arrangement on the B/B′-sites, whereas Mn occupy the highly distorted cuboctahedra voids at the A sites. A small Mn-Sc cation inversion was reported in a previous NPD study of the x = 0 structure.[21] NPD data for the present Co-substituted samples show that substantial cation disorder is present at both the A and B sites of the $A_2BB'O_6$ DPv structure, although B′ was found to be occupied only by Sb in all samples. The neutron scattering lengths (Mn/Co/Sc = −3.73/2.78/12.1 fm) provide good scattering contrast, but the populations of the three metals over their two sites cannot be determined uniquely without imposing constraints on composition. The relative cation sizes (6-coordinate (high spin) ionic radii for $Mn^{2+}/Co^{2+}/Sc^{3+}$ are 0.83/0.745/0.745 Å) show that Co^{2+} should more easily substitute for Sc^{3+} than for Mn^{2+}, and furthermore Co^{2+} gains crystal field stabilisation at the octahedral B-site, hence we have assumed that Co^{2+} initially substitutes for Sc^{3+} at the B-sites, with displaced Sc^{3+} mixed with Mn^{2+} at the A-sites, *i.e.* distribution $(Mn_{2-x}Sc_x)(Sc_{1-x}Co_x)SbO_6$ for $0 < x < 1$. Refining Mn/Sc and Co/Sc populations at the A and B sites respectively gives composition $(Mn_{0.748(3)}Sc_{0.252(3)})_2(Co_{0.460(7)}Sc_{540(7)})SbO_6$ for the x = 0.5 sample, in good agreement with this simple model, and the overall refined composition of $Mn_{1.50(1)}Co_{0.46(1)}Sc_{1.04(1)}SbO_6$ is in excellent agreement with the ideal stoichiometry. Mn^{2+} and Co^{2+} charges are assigned based on charge balance of this composition. Oxygen site occupancies were refined in initial neutron diffraction analysis, but no significant oxygen deficiency was found. For compositions with $1 < x < 2$, the above model would predict the B-site to be occupied only by Co, and with Mn, Sc and Co mixed at the A-site, *i.e.* $(Mn_{2-x}ScCo_{x-1})(Co)SbO_6$ for $1 < x < 2$. However, NPD refinement revealed Sc occupancy at the B-site for x = 1.0 and 1.5 samples, and so these were refined with Mn/Sc/Co at the A-site and Co/Sc at the B-site, constrained to the ideal stoichiometry. B-sites were found to have near 50 : 50 populations of Co and Sc as shown in Fig. 3a and b, so the cation distribution may be written as approximately $(Mn_{2-x}Sc_{0.5}Co_{x-0.5})(Sc_{0.5}Co_{0.5})SbO_6$ for $0.5 < x < 2$. The corresponding average A and B site to O distances across the series are in Fig. 3c and d. A systematic shortening of the A–O bond length with increasing x is observed, consistent with replacement of Mn^{2+} by smaller Co^{2+} and Sc^{3+}, and this also leads to increasing monoclinic β angles and in-phase rotation of the (Sc/Co)/SbO_6 octahedra along the c axis (c^+ tilt) as shown in Fig. 2b. Results for the refined crystal structures are in Tables S1–S3 in SI.

Zero-field cooled magnetic susceptibility data from the three $Mn_{2-x}Co_xScSbO_6$ samples (x = 0.5, 1 and 1.5) under an applied magnetic field of 0.1 T are shown in Fig. 4a–c. All samples show a Curie transition at $T_C \approx 50$ K which NPD data below show is due to an NTO-type secondary phase. The x = 0.5 sample also shows a prominent transition consistent with antiferromagnetic (AFM) order at T_N = 18 K, corresponding to the long-range A-site AFM order of the DPv phase as found from NPD below. This transition broadens and shifts to lower temperature with increasing x at 1 and 1.5, indicating increasingly short-range or glassy magnetic behaviour, consistent with the later NPD results, although AC susceptibility measurements would be needed to confirm a spin glass transition. As well as the NTO-type secondary phase, the refinements reveal $Sc_{5.5}Sb_{1.5}O_{12}$ and rocksalt type (Mn/Co)O impurities, but as the former is non-magnetic and the latter order magnetically at much higher temperatures, they do not account for the observed low-temperature anomalies. The weak broad anomaly with a small field dependence observed in the heat capacity (Fig. 4d and e) are also consistent with a probable spin freezing transition in the x = 1 sample.

Magnetisation-field (M–H) loops at 5 K for all samples are shown in Fig. 4f. The nearly linear variations and lack of

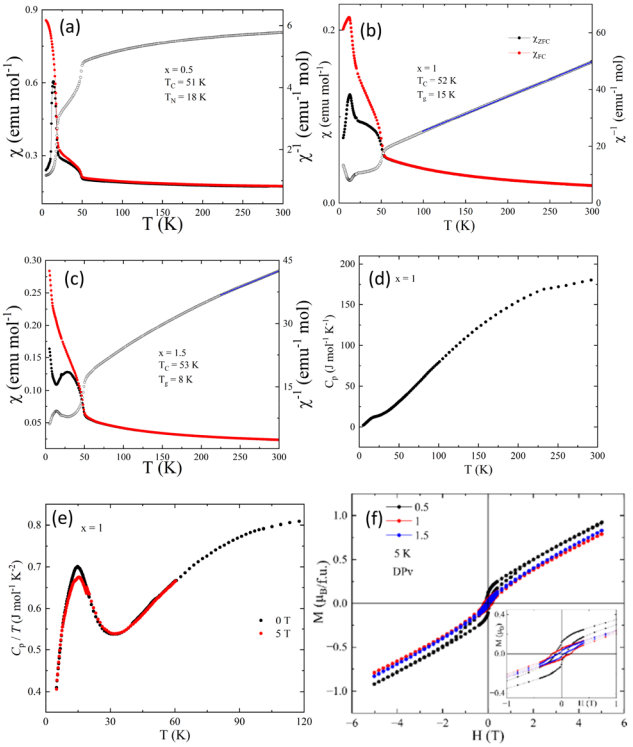

Fig. 4 Magnetic susceptibilities collected at 0.1 T after zero-field cooling (ZFC, black points) and field cooling (FC, red points) for HPHT-synthesised $Mn_{2-x}Co_xScSbO_6$ samples; (a) x = 0.5, (b) x = 1.0, (c) x = 1.5. Curie–Weiss fits to the high temperature inverse FC susceptibilities are shown in (b) and (c). Values of the Curie transition T_C from NTO-type secondary phases and intrinsic antiferromagnetic (T_N) or probable spin glass (T_g) transitions are also shown. (d) Heat capacity (C_p) as a function of temperature for the x = 1 sample, and (e) the derived low temperature C_p/T variations under 0 and 5 T fields. (f) Magnetisation-field (M–H) hysteresis loops at 5 K with the low field region expanded in the inset. x = 0.5 shows a weak hysteretic component superimposed on a largely linear M–H response at 5 K, whereas x = 1 and 1.5 exhibit glassy magnetic behaviour consistent with spin-freezing.

saturation in the M–H loop of x = 0.5 is consistent with predominantly antiferromagnetic interactions in the DPv phase. The ferromagnetic hysteresis with small remanent magnetisation (M_r = 0.11 μ_B) and coercive field (H_c = 0.10 T) likely arise from the secondary NTO polymorph phase. For x = 1 and 1.5 M–H loops, the nearly linear combinations of magnetisation and applied magnetic fields with negligibly small M_r and H_c are consistent with short-range spin ordering. Room temperature M–H results are summarised in Fig. S4 in ESI.

Low temperature NPD data were collected from the three DPv $Mn_{2-x}Co_xScSbO_6$ samples (x = 0.5, 1 and 1.5) at temperatures between 1.5 and 80 K (Fig. S5) to investigate low temperature spin ordering. Variable-temperature NPD data of x = 0.5 in Fig. 5a and Fig. S6 show additional magnetic peaks below 50 K at 2θ = 31° and 33°, and further reflections at 2θ = 25° and 45° below 18 K. The magnetic peaks appearing below 50 K are indexed on the cell of the 8% NTO-type secondary phase, where spin ordering with propagation vector k = [0 0 0] gives magnetic intensities on top of the nuclear reflections. Magnetic peaks

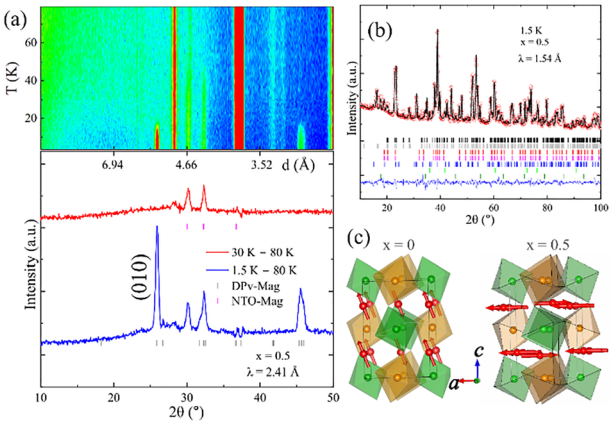

Fig. 5 (a) Variable temperature NPD data and difference patterns (30–80 K and 1.5–80 K) showing the two magnetic transitions. Magnetic peaks with grey/pink tick marks represent the DPv/NTO-type phases, respectively. (b) Rietveld fit to the NPD data of x = 0.5 at 1.5 K. The tick marks from top to bottom represent DPv-nuclear, DPv-magnetic, NTO-nuclear, NTO-magnetic, $Sc_{5.5}Sb_{1.5}O_{12}$, (Mn,Co)O-nuclear, and (Mn,Co)O-magnetic phases, respectively. (c) Magnetic structures of DPv-$Mn_{2-x}Co_xScSbO_6$ (x = 0, 0.5) with propagation vector k = [0 0 0] and antiferromagnetic ordering.

emerging below 18 K are indexed on the DPv phase as denoted in Fig. 5a. The magnetic structure was fitted to 1.5 K high resolution NPD data for x = 0.5 as shown in Fig. 5b. Magnetic peaks from the rocksalt (Mn,Co)O impurity were also fitted. DPv-Mn_2ScSbO_6 (x = 0) was previously found to have a k = [0 0 0] A-site antiferromagnetic spin order with Mn^{2+} spins oriented in the ac-plane with component along the c-axis of 4.26(1)μ_B and along the a-axis of 1.58(1)μ_B, resulting in a total moment of 4.54(1)μ_B, as shown in Fig. 5c.[21] This spin structure is characterised by strong (010) and (100) magnetic NPD intensities. The magnetic reflections for x = 0.5 are also indexed with the propagation vector k = [0 0 0], but magnetic (100) intensity is absent indicating that the spin orientation is different to x = 0. NPD fits showed that the magnetic structure can be described as an antiferromagnetic arrangement of spins parallel to the a-axis with a moment of 2.92(3)μ_B, as exhibited in Fig. 5c. The A-site moment reduction from the spin-only expectation of 3.75 μ_B for $(Mn_{2-x}Sc_x)(Sc_{1-x}Co_x)SbO_6$ with x = 0.5 reflects disorder from dilution of Mn^{2+} by non-magnetic Sc^{3+}. No long-range order of the B-site Co-spins was observed, presumably because these are more highly diluted. Refined crystal and magnetic parameters are shown in Table 1.

No magnetic reflections are observed in NPD data collected from the x = 1 and 1.5 samples down to 1.5 K (Fig. S7), demonstrating an absence of long-range magnetic ordering. For x = 1, comparison of the NPD patterns collected at 1.5 K and 80 K reveals a broad low-angle scattering enhancement centred around 2θ = 18°, consistent with short-range magnetic correlations. However, the corresponding comparison for x = 1.5 shows no low-angle feature, suggesting that magnetic correlations are further suppressed in this composition. Together with the ZFC/FC bifurcation, these observations suggest a glass-like magnetic ground state in the x = 1 and x = 1.5

Table 1 Crystal structure and magnetic parameters for DPv $Mn_{2-x}Co_xScSbO_6$, showing synthesis pressure, monoclinic lattice parameters, antiferromagnetic and spin-freezing transition temperatures (T_N and T_g), the magnetic frustration factor (f), Weiss temperature (θ) and effective moment (μ_{eff}) obtained from Curie–Weiss fits, and the ordered A-site moment. Data for x = 0 is from ref. 19

x	P (GPa)	a (Å)	b (Å)	c (Å)	β (°)	T_N; T_g[a] (K)	f	θ (K)	μ_{eff} (μ_B)	M (μ_B)
0	12	5.2909 (3)	5.4698 (3)	7.7349 (5)	90.165 (6)	22.3	4.2	−94	7.8	4.54(1)
0.5	6	5.2804 (5)	5.4443 (2)	7.7221 (3)	90.284 (4)	18				2.92(3)
1	6	5.2661 (3)	5.4160 (2)	7.7032 (4)	90.412 (3)	15[a]	7.2	−108	8.1	
1.5	6	5.2524 (2)	5.3811 (2)	7.6861 (3)	90.571 (3)	8[a]	26.6	−213	9.4	

Note: The Curie–Weiss equation could not be reliably fitted to data for x = 0.5 data due to magnetic impurity.

samples, most likely involving spin freezing within these cation-disordered DPv phases. Rietveld fits for x = 1 and 1.5 to 1.5 K NPD data are presented in Fig. S8 in ESI.

The results above demonstrate that Co-doped $A_2BB'O_6$ double perovskites $Mn_{2-x}Co_xScSbO_6$ have been synthesised for x = 0.5, 1 and 1.5 at 6 GPa pressure. The decrease in unit-cell parameters with increasing x (Fig. 2a) confirms that Co^{2+} has been incorporated into the lattice in place of Mn^{2+}. The outline P–T phase diagram in Fig. 6 highlights the stabilisation of the DPv phase at pressures ~6 GPa: the x = 0 composition Mn_2ScSbO_6 adopts the NTO structure at 5.5 GPa and transforms to DPv at 12 GPa,[21] while Co_2ScSbO_6 (x = 2) shows only an NTO-type phase with no DPv structure observed at 12 GPa synthesis pressure.[22] In contrast, all of the intermediate $Mn_{2-x}Co_xScSbO_6$ compositions investigated here (x = 0.5, 1, 1.5) form a majority DPv phase at 6 GPa synthesis pressure. This behaviour is consistent with entropy (disorder) stabilisation of the DPv phase arising from substantial cation mixing and configurational complexity. While configurational entropy is likely to be important in governing phase stability, variations in kinetic trapping from HPHT synthesis conditions and structural effects may also influence the observed phase selection. Perovskites in general are known to be compositionally flexible, and here the DPv structure can accommodate $Mn^{2+}/Co^{2+}/Sc^{3+}$ cations at both the cuboctahedral A-site cavities and the octahedral B sites. Although there is some tendency for Co^{2+} to occupy the B-site based on size and crystal field factors, it is notable that the cation populations for the three investigated samples all have near 50 : 50 Co : Sc occupancy of the B-site, and with remaining cations mixed at the A-site networks according to stoichiometry, *i.e.* cation distribution ~$(Mn_{2-x}Sc_{0.5}Co_{x-0.5})$-$(Sc_{0.5}Co_{0.5})SbO_6$ for 0.5 < x < 1.5. The 50 : 50 mix of Co^{2+}/Sc^{3+} cations (of identical ionic radius) gives maximal configurational entropy without strains induced by changing the average B-cation size, while mixing of two or three cations at the A-sites provides further disorder entropy for x = 0.5, 1 and 1.5. This configurational disorder stabilises the chemically complex DPv at a relatively low synthesis pressure of 6 GPa for x = 0.5, 1 and 1.5. Formation of $Mn_{2-x}Co_xScSbO_6$ (0.5 < x < 1.5) at 6 GPa thus represents a notable example of a high-pressure DPv system whose stabilisation is consistent with a substantial cation disorder (entropy) contribution.

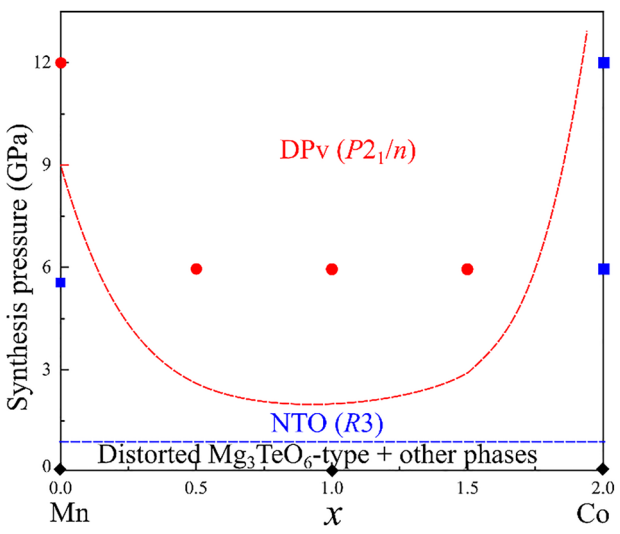

Fig. 6 Schematic summary of the phases obtained for $Mn_{2-x}Co_xScSbO_6$ under the pressure–temperature synthesis conditions explored. Red/blue/black symbols show samples that predominantly contained DPv/NTO-type/Mg_3TeO_6-type and other phases.

Disorder from mixing two magnetic cations with different d-electron configurations plus dilution with non-magnetic Sc^{3+} cations at both A- and B-sites disrupts the long-range spin antiferromagnetic order previously reported for x = 0.[21] This is evidenced by decreasing Néel or freezing transition temperatures and increasing magnetic frustration factors with increasing x as shown in Table 1. The x = 0.5 sample is found to retain the antiferromagnetic k = [0 0 0] spin structure of the x = 0 material, but with magnetic moments reduced in magnitude and rotated by ~70° to lie parallel to the a-axis. Upon further Co substitution (x = 1 and 1.5), magnetic Bragg diffraction is suppressed and the broad low-angle feature observed for x = 1 is consistent with short-range or glassy magnetic correlations.

Conclusion

This investigation of the $Mn_{2-x}Co_xScSbO_6$ system at 6 GPa synthesis pressure has shown that, unexpectedly, a double perovskite phase is stabilised across the 0.5 < x < 1.5 range, despite the x = 0 and x =2 members forming a different, NTO-type, structure at comparable pressure. This behaviour is consistent with disorder (entropy) stabilisation of the intermediate compositions under the reported HP synthesis conditions, and neutron diffraction studies reveal substantial disorder at both the A and B sites of the $A_2BB'O_6$ double perovskite structure

following approximate composition $(Mn_{2-x}Sc_{0.5}Co_{x-0.5})$-$(Sc_{0.5}Co_{0.5})SbO_6$ for $0.5 < x < 1.5$. The long range antiferromagnetic order previously reported for $x = 0$ is increasingly suppressed by Co-doping. The $x = 0.5$ sample exhibits long-range antiferromagnetism with ordered moments rotated and reduced in magnitude relative to $x = 0$, whereas $x = 1$ and 1.5 show low-temperature glassy magnetic behaviour associated with spin-freezing, without observed long-range magnetic order. This study thus demonstrates that interesting new magnetic materials may be accessed through a combination of high pressure synthesis and entropic stabilisation of cation-disordered phases.

Author contributions

This study was designed by KJ, JPA and YS. Experimental work and data analysis was performed by KJ, FDR and CR. The paper was written by KJ, JPA and YS with contributions from all authors.

Conflicts of interest

There are no conflicts to declare.

Data availability

The data supporting this article have been included as part of the supplementary information (SI). The supplementary information includes XRD Data, magnetisation measurement analysis and NPD refinement results. See DOI: https://doi.org/10.1039/d6tc00432f.

Data for this article, including structural and magnetic data are available at https://datashare.ed.ac.uk/handle/10283/838.

Acknowledgements

This work was partly supported by Grants-in-Aid for Scientific Research (No. 20K20547, 20H00397, 22KK0075, and 23H05457), and by a grant for the International Collaborative Research Program of the Institute for Chemical Research in Kyoto University from MEXT of Japan. Support was also provided by Advanced International Collaborative Research Program (AdCORP), grant No. JPMJKB2304, Adopting Sustainable Partnerships for Innovative Research Ecosystem (ASPIRE), grant No. JPMJAP2314, by the Japan Science and Technology Agency (JST), and EPSRC, UK.

References

1 M. Imada, A. Fujimori and Y. Tokura, *Rev. Mod. Phys.*, 1998, **70**, 1039–1263.
2 E. Dagotto, *Science*, 2005, **309**, 257–262.
3 J. B. Goodenough, *Rep. Prog. Phys.*, 2004, **67**, 1915–1993.
4 N. A. Hill, *J. Phys. Chem. B*, 2000, **104**, 6694–6709.
5 J. V. Badding, *Annu. Rev. Mater. Res.*, 1998, **28**, 631–658.
6 W. T. Chen, M. Mizumaki, H. Seki, M. S. Senn, T. Saito, D. Kan, J. P. Attfield and Y. Shimakawa, *Nat. Commun.*, 2014, **5**, 3909.
7 X. Wang, M. Liu, X. Shen, Z. Liu, Z. Hu, K. Chen, P. Ohresser, L. Nataf, F. Baudelet, H.-J. Lin, C.-T. Chen, Y.-L. Soo, Y.-F. Yang, C. Jin and Y. Long, *Inorg. Chem.*, 2019, **58**, 320–326.
8 Y. W. Long, N. Hayashi, T. Saito, M. Azuma, S. Muranaka and Y. Shimakawa, *Nature*, 2009, **458**, 60–63.
9 M. Azuma, W.-T. Chen, H. Seki, M. Czapski, O. Smirnova, K. Oka, M. Mizumaki, T. Watanuki, N. Ishimatsu, N. Kawamura, S. Ishiwata, M. G. Tucker, Y. Shimakawa and J. P. Attfield, *Nat. Commun.*, 2011, **2**, 347.
10 Z. Tan, J. A. Lussier, T. Yamada, Y. Xu, T. Saito, M. Goto, Y. Kosugi, D. Vrublevskiy, Y. Kanemitsu, M. Bieringer and Y. Shimakawa, *Angew. Chem., Int. Ed.*, 2022, **61**, e202203669.
11 H. L. Feng, C.-J. Kang, B. Kim, K. Kim, M. Croft, S. Liu, T. A. Tyson, E. Stavitski, R. Zu, V. Gopalan, S. H. Lapidus, C. E. Frank, Y. Shi and M. Greenblatt, *Chem. Mater.*, 2021, **33**, 6522–6529.
12 S. Vasala and M. Karppinen, *Prog. Solid State Chem.*, 2015, **43**, 1–36.
13 (*a*) A. M. Arévalo-López, G. M. McNally and J. P. Attfield, *Angew. Chem., Int. Ed.*, 2015, **54**, 12074–12077; (*b*) M.-R. Li, M. Retuerto, Z. Deng, P. W. Stephens, M. Croft, Q. Huang, H. Wu, X. Deng, G. Kotliar, J. Sánchez-Benítez, J. Hadermann, D. Walker and M. Greenblatt, *Angew. Chem., Int. Ed.*, 2015, **54**, 12069–12073.
14 K.-I. Kobayashi, T. Kimura, H. Sawada, K. Terakura and Y. Tokura, *Nature*, 1998, **395**, 677–680.
15 D. D. Sarma, P. Mahadevan, T. Saha-Dasgupta, S. Ray and A. Kumar, *Phys. Rev. Lett.*, 2000, **85**, 2549–2552.
16 S. Ray, A. Kumar, D. D. Sarma, R. Cimino, S. Turchini, S. Zennaro and N. Zema, *Phys. Rev. Lett.*, 2001, **87**, 097204.
17 Y. S. Oh, X. Luo, F.-T. Huang, Y. Wang and S.-W. Cheong, *Nat. Commun.*, 2014, **5**, 3201.
18 M.-R. Li, E. E. McCabe, P. W. Stephens, M. Croft, L. Collins, S. V. Kalinin, Z. Deng, M. Retuerto, A. Sen Gupta, H. Padmanabhan, V. Gopalan, C. P. Grams, J. Hemberger, F. Orlandi, P. Manuel, W.-M. Li, C.-Q. Jin, D. Walker and M. Greenblatt, *Nat. Commun.*, 2017, **8**, 2037.
19 J. A. Alonso, M. J. Martínez-Lope, M. T. Casais and M. T. Fernández-Díaz, *Inorg. Chem.*, 2000, **39**, 917–923.
20 S. A. Ivanov, P. Nordblad, R. Mathieu, R. Tellgren, E. Politova and G. André, *Eur. J. Inorg. Chem.*, 2011, **2011**, 4691–4699.
21 E. Solana-Madruga, A. J. Dos Santos-García, A. M. Arévalo-López, D. Ávila-Brande, C. Ritter, J. P. Attfield and R. Sáez-Puche, *Dalton Trans.*, 2015, **44**, 20441–20448.
22 K. Ji, E. Solana-Madruga, A. M. Arévalo-López, P. Manuel, C. Ritter, A. Senyshyn and J. P. Attfield, *Chem. Commun.*, 2018, **54**, 12523–12526.
23 J. Rodríguez-Carvajal, *Phys. B*, 1993, **192**, 55–69.
24 J. Rodríguez-Carvajal, *BASIREPS*: *a program for calculating irreducible representations of space groups and basis functions for axial and polar vector properties*, *Part of the FullProf Suite of programs*, Institut Laue–Langevin, Grenoble, France, available at https://www.ill.eu/sites/fullprof/.
25 A. M. Glazer, *Acta Cryst.*, 1972, **B28**, 3384–3392.

